A Thesis

On

Performance of dye-sensitized solar cell based on metal-deposited $BiFeO_3$ nanoparticles

(Submitted in the partial fulfillment of requirement for the award of the degree of)

Master of Science (Physics)

Submitted by

Imanpreet Kaur

Roll No: 301104007

Supervisor

Dr. N.K. Verma

Senior Professor

Under

School of Physics & Materials Science

Thapar University, Patiala (Punjab) - 147004

July 2013

Dedicated to my

Parents & Teachers

Certificate

This is to certify that the thesis entitled **"Performance of Dye-sensitized solar cell based on metal-deposited $BiFeO_3$ nanoparticles"** submitted by **Imanpreet Kaur, Roll no. 301104007** in the partial fulfillment of the requirement for the award of the degree **Master of science in Physics,** from the School of Physics and Materials Science, Thapar University, Patiala -147 004, is a record of candidate's own work carried out by her under my supervision and guidance. She has not submitted this material for credit towards any other degree at Thapar University, Patiala or any other University.

(Dr. N.K.Verma)
Senior Professor
School of Physics and Materials Science
Thapar University, Patiala-147004 (Punjab)

Countersigned by:

(Dr.Kulvir Singh)

Head and Professor
School of Physics and Materials Science
Thapar University, Patiala-147004(Punjab)

(Dr. S. K. Mohapatra)

Dean of Academic Affairs
Thapar University, Patiala-147004(Punjab)

Acknowledgment

I express my sincere thanks to my esteemed and worthy supervisor **Dr. N.K. Verma, Senior Professor, School of Physics and Materials Science, Thapar University** for his valuable guidance in carrying out this work under his effective supervision, encouragement, enlightens and cooperation. I would have never succeeded in completing my task without the cooperation, encouragement and help provided to me by various personalities.

I shall be failing in my duties if I do not express my deep sense of gratitude towards **Dr. Kulvir Singh,** Head and Professor, School of Physics and Materials Science**,** who has been a constant source of inspiration for me throughout this work.

I express my cordial thanks especially to **Mr. Gurmeet Singh Lotey** and **Miss Kamaldeep Kaur** for their ever available guidance and indispensable comments, which helped me to develop and shape this study in the present form.

I am also thankful to Miss Manveen Kaur, Mr. Jaspal Singh, Miss Lavanya Khanna, and Miss Gitanjali Dhir.

I would like to express my deepest gratitude to **my parents**, without whom I am nothing, to provide me great opportunities, everlasting support, big encouragement and lots of love.

Above all I render my gratitude to the **ALMIGHTY**, who bestowed self-confidence, ability and strength in me to complete this work.

Imanpreet Kaur

(Imanpreet Kaur)

(301104007)

Abstract

The supply of clean, green and environment friendly energy to our society is a matter of great concern for the scientific communities, as the non-renewable resources such as gas; coal and oil are limited and for sure will run out with time. Solar energy is one of the most promising alternative energy resources. Therefore, today much attention has been paid on dye-sensitized solar cells (DSSCs) in the both academic and industrial platforms as an alternative clean and green energy resource precisely because of their relatively high energy conversion efficiency, low production cost, low manufacturing toxicity, ease of fabrication and flexibility. Advances in this field have been achieved by improving the energy conversion efficiency, by extensively studying the mechanism to enhance electron generation, injection or transfer to semiconductors and reduction in the charge recombination processes.

In the light of above, in the present study DSSC has been fabricated using bare and Au decorated $BiFeO_3$ nanoparticles. The synthesized nanoparticles show excellent energy conversion efficiency around 2.99%. The synthesized materials have wide range of application in the futuristic photovoltaic devices.

List of figures

Contents

Chapter 1
Introduction

1.1 Nanoscience and Nanotechnology

Nanomaterials based systems and devices have attracted huge interests from the researchers over the past few decades. The word nanoscience refers to the study, manipulation and engineering of matter, particles and structures on the nanometer scale (one millionth of a millimeter, the scale of atoms and molecules). Nanotechnology is the application of nanoscience leading to the use of new nanomaterials and nano-size components in useful products. Nanotechnology will eventually provide us with the ability to design custom-made materials and products with new enhanced properties, new nanoelectronics components, new types of "smart" medicines and sensors, and even interfaces between electronics and biological systems [1].

Nanomaterials are of special interests to the materials-research community, due to their potential applications in catalysis, biomedicines, and electronics. Probably unbeknownst to us, nanomaterials have become part of our everyday lives. The research of nanomaterials focuses on the creation and exploitation of materials which have morphological characteristics from atoms to bulk materials and with at least one dimension in the nanoscale range [2-4].

The increasing energy demand in the near future will force us to seek environmentally clean alternative energy resources. Presently, our society is based on coal, oil and natural gas as a source of energy, but these fossil fuels are depleting at a fast rate, due to their limited availability. Moreover, carbon dioxide is produced in the combustion of fossil fuels and the rapid increase of carbon dioxide concentration has resulted in global warming effects. Biggest challenge for our global society is to find ways to replace the slowly but inevitably vanishing fossil fuel supplies by renewable Green energy resources and, at the same time, avoid negative effects from the current energy system on climate, environment, and health. Therefore, the need of hour is to find environmental friendly solution of energy problems and to utilize maximum natural sources by various ways. Some of the possible sources are fuel cells, photovoltaic devices, wind power generators and geothermal power generators.

To solve the problem of energy crisis solar energy is expected to play a crucial role as a future Green energy source. The sun provides a power of about 1,20,000 TW to the earth's surface, which amounts to 6000 times the present rate of the world energy consumption. One area of great promise is conversion of solar energy to electricity, with the help of photovoltaic cells, as it silently generate electricity and does

not produce air pollution or hazardous waste. Current solar power technology has little chance to compete with fossil fuels or large electric grids. Hence, it is essential to tap the other sources of energy to supplement the existing energy demands of all non-conventional energy sources. Solar energy holds the greatest promise as it is abundant, renewable and pollution free. Its collection, storage on conversion is also easy. Hence, worldwide attention is now focused on various methods of utilization of solar energy.

Photovoltaic cells convert light energy directly into electricity. They are often called solar cells because the source of light is usually the sun. Traditionally, solar cells were used as the key part of panel systems that generated electricity or heat for homes. These days, the technology is used in a wide variety of applications, which means the style of solar cells vary per application.

Different generations of solar cell technology have been identified in the solar cell industry:

First Generation solar cells: The first generation includes Silicon wafer based photovoltaic cells, having a quite high efficiency. These are approaching their theoretical efficiency maximum of 33%. In 2007, first generation solar cells accounted for 89.6% of commercial production. These solar cells are configured as a large-area-p-n junction made by diffusing an n- type dopant into a p-type wafer or vice-versa. The manufacturing processes that are used to produce first generation cells are inherently expensive. The first generation cells will not be able to provide more cost effective energy than fossil fuel sources [5].

Second Generation solar cells: The second generation solar cells are also called thin-film solar cells, for example, amorphous silicon, Copper Indium Gallium Diselenide, Cadmium Telluride. The advantage of the second generation is that, they are low in cost and flexible whether they exhibits less efficiency of 20% . However, these materials have poor stability, and are difficult to manufacture in large areas while maintaining the required material quality and low cost [5].

Third Generation solar cells: Solar cells are the leading edge of solar technology. Third generation cells include solar cells that do not need the p-n junction, which are necessary in silicon-based cells. Still in the research phase, third generation cells have moved well beyond silicon-based cells [6].

One important concept to reduce the solar cell cost and to increase the conversion efficiency is to use nanotechnology; i.e., to use the nanostructured material in solar cells. Materials scientists have found that it is possible to design photovoltaic solar cells using nanotechnology-based semiconductor materials including nanowires, nanocrystals, nanorods, nanodots, etc [7].

Summarizing various generations of solar cells we find that first generation devices suffer from high cost of manufacturing and installation. The second generation devices consisting of polycrystalline semiconductor thin films can bring down the price significantly, but their efficiency needs to be enhanced

in order to make them practically viable. Now being aimed are the third generation devices that can deliver high efficiency devices at an economically viable cost. The ability to design nanostructured semiconductors, organic-inorganic hybrid assemblies, and molecular assemblies opens up new ways to design such third generation light energy conversion devices. The emergence of nanomaterials as the new building blocks to construct light energy harvesting assemblies has opened up new ways to utilize renewable energy sources. The motivations to employ nanostructures in solar cells are largely divided into three categories first, to improve the performance of conventional solar cells, second, to obtain relatively high conversion efficiency from low grade (inexpensive) materials with low production cost and low-energy consumption, third, to obtain conversion efficiency higher than the theoretical limit of conventional p–n junction solar cell [8].

Third generation contains a wide range of potential solar innovations including polymer solar cells, nanocrystalline cells, and dye-sensitized solar cells. Those may overcome the fundamental limitations of photon to electron conversion in single-junction devices and, thus, improve both their efficiency and cost. These nanocrystalline photovoltaic devices, which were invented in the early 1990s, promise viable solutions to future large-scale solar-energy conversion issues on the bases of cost, efficiency, stability, availability, and environmental compatibility. To fully realize the potential of these various types of next-generation solar cells, it is critical to perform both basic and applied research into new technologies.

1.2 Photovoltaic devices based on nanostructural materials

Nanostructure-based photovoltaic (PV) cells have been previously proposed due to their potential to provide high-energy conversion efficiency. The large energy conversion efficiency arises from the following effects:

i. Nanostructure crystallite sizes are comparable to the carrier scattering lengths, this significantly reduces the scattering rate, thus increasing the carrier collection efficiency

ii. Nanostructures have strong absorption coefficient due to increased density of states. In addition, by varying the size of the nanostructures, the band gap can be tuned to absorb in a particular photon energy range.

iii. Size-dependent properties of nanostructures such as quantum size effects in semiconductor nanoparticles provide the basis for developing newer and effective systems.

In contrast to the conventional systems where the semiconductor assume both the task of light absorption and charge carrier transport the two functions are separated here. DSSC consists of the meso-porous oxide layer of semiconductor on glass substrate Fluorine doped Tin oxide (FTO) composed of nanometer-sized particles which acts as an anode on which dye molecules gets adsorbed; counter electrode generally coated with platinum as a catalyst which acts a cathode; electrolyte containing redox couple I-/I3- sandwiched between two electrodes.

1.3 Dye-Sensitized Solar Cells (DSSC)

Amongst these various solar cells, there is a boost in dye-sensitized solar cells which provide a technically and economically credible alternative concept to present day p–n junction photovoltaic devices. DSSC captured the attention of the international research community in 1991 with the report of a 7% efficient cell by O'Regan and Grätzel. The efficiency of DSSC has increased considerably in last 20 years, with the confirmed record now standing at 11% [9]. Unlike the crystalline and thin film solar cells that have solid-state light absorbing layers, dye sensitized solar cells is composed of a dye adsorbed semiconductor (TiO2, ZnO, SnO2, etc.) electrode, a liquid electrolyte containing the redox couple I-/I3- sandwiched between glasses having transparent conductive oxide layer as shown in Figure 1.1. The DSSC consist of senstizing dye, nanoparticles, and electrolyte. The mechanism of the dye sensitized solar cell has three steps:

i. A dye, adsorbed on a layer of semiconductor interacts with the visible light provided by the sun (just like the green pigment does in a leaf), promoting an electron from a lower level orbital to an excited one. Photo-excitation occurs when the photons from the light source penetrate the solar cell to excite the dye's electrons.

ii. The excited electron is injected by the dye into the semiconductor and, the chemical diffusion of electrons from the semiconductor layer into the FTO/ITO conductive layer occurs when the multi-meter is connected creating the outside circuit.

iii. The electrons return to the cell to complete the circuit and bring the dye back to its "normal" state by using an electrolyte solution that helps carry electrons through the cell.

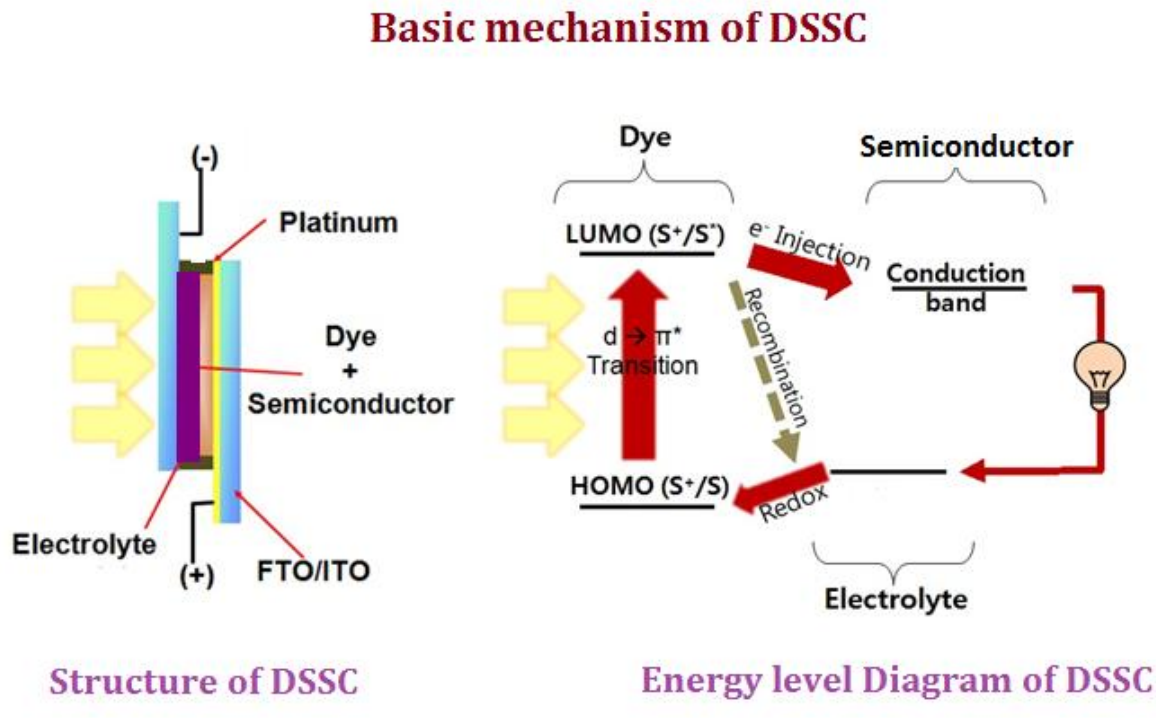

Figure 1.1: Basic structure and working mechanism of a Dye- Sensitized Solar Cell

The illumination of fabricated DSSC results in photo-excitation of the dye takes place. This results in the injection of electrons to the conduction band of the semiconductor. The original state of the dye is subsequently restored by electron donation from the electrolyte. The regeneration of the sensitizer by the electrolyte intercepts the recapture of the conduction band electron of the oxidized dye. The current is generated in turn at the counter electrode and the circuit is completed via electron migration through the external load. DSSCs have attracted much attention as they offer the possibility of extremely inexpensive and efficient solar energy conversion.

1.4 Applications of DSSCs

i. The first commercial shipment of low-light, ultra thin, solar cell technology called DSSC, created by G24 Innovations, has been sent to Hong Kong-based consumer electronics bag manufacturer, Mascotte Industrial Associates for use in backpacks and bags.

ii. DSSC is ideal for clothing and portable applications, DSSCs are less than 1mm thick, inexpensive, don't contain silicon or cadmium and can even operate indoors, making them ideal for powering cell telephones, cameras and portable electronics.

iii. DSSCs also can be embedded into tent material to power LED lighting systems for camping.

Chapter-2

Literature Review

The literature has been reviewed in detail, in order to gain optimum information as well as to the genesis, and technical applications of the research work:

DSSC proposed by O'Regan and Grätzel [10] has attracted substantial interest since 1991, due to its characteristics, such as low production cost, and low environmental impact during fabrication.

The need for DSSC to absorb far more of the incident light was the driving force for the development of mesoscopic semiconductor materials with an enormous internal surface area. Various semiconductors such as TiO_2 [11] $BaTiO_3$ [12], SnO_2 [13], ZnO [14], Nb_2O_5 [15], and Zn_2SnO_4 [16] have been used as an anode material, are relatively wide band gap materials and generally transparent to visible light. Narrow band gap materials such as GaAs, Fe_2O_3 and CdS get easily corroded in contact with the electrolyte. Among these anode materials ZnO and TiO_2 having wide band gap are suitable materials for DSSC due to their excellent electrochemical stability [17].

The major breakthrough in DSSC was the use of a high surface area nanoporous TiO_2 layer, which has achieved highest efficiency of 11%. A single monolayer of the dye on the semiconductor surface was sufficient to absorb essentially all the incident light in a reasonable thickness (several μm) of the semiconductor film. TiO_2 is most appropriate candidate for DSSC due to its peculiar and fascinating properties such as large band gap, economical, abundant, and non-toxic [18].

Several methods have been utilized to modify the structure of the working electrode to improve the performance of the DSSC [19]. Different morphologies such as nanoparticles [20], nanowire arrays [21], nanotubes [22], nanofiber mats [23], nanoflowers [24], ellipsoidal shaped nanoparticles [25], spiral shaped wires [26] and tetrapods [27] of TiO_2 have been employed as photoanode in fabrication of DSSC. It is now well-accepted that a high-efficiency photo electrode for DSSCs requires not only a high surface area for the loading of large amounts of dye molecules but also a tailored microstructure for light harvesting and fast electron transport.

Increasingly research into DSSC is addressing the use of more sophisticated device architectures in order to reduce interfacial recombination losses. To improve the overall cell performance of DSSCs, attempts have been made to retard back transfer of photo induced electrons through the TiO_2/dye/electrolyte interface by surface modification of TiO_2 using insulating metal oxides and hydroxides or high band gap semiconductors that form a blocking layer between the dye sensitizer and semiconductor layer to block the back electron flow towards the electrolyte species. One particularly attractive approach involves the coating of the semiconductor (TiO_2) film with a thin overcoat of another metal oxide with a higher conduction band edge. Over the past decade, many studies have been found on the effect of core/shell structures on the performance of DSSC including TiO_2/ZnO [28] TiO_2/ZrO_2 [29], TiO_2/In_2O_3 [30], TiO_2/SnO_2 [31], TiO_2/Nb_2O_5 [32], $TiO_2/SrTiO_3$ [33], TiO_2/Al_2O_3 [34], $TiO_2/CaCO_3$ [35].

In DSSCs, at the semiconductor/electrolyte interface, the recombination of a portion of the electrons is still inevitable. There are several studies to decrease this undesired reaction at the interface of semiconductor/electrolyte by using core-shell structure of various metal oxides or by using different additives in the electrolyte to passivate the exposed electrolyte. There are few reports showing that addition of noble metal nanoparticles improves DSSC energy conversion efficiency. With the deposition of noble metals, a Schottky barrier is formed in the interfacial region of the metal and the semiconductor, reducing the electron hole recombination, thus the electron injection efficiency gets increased. Moreover, the unique property of metal nanoparticles i.e. Surface plasmon resonance also plays a vital role in improving the performance of DSSC. So, with this point of view high efficiency can be anticipated using the combination of noble metal/TiO_2 nanostructures for DSSC application.

2.1 Bismuth Ferrite nanostructures as photoactive semiconductor

The energy band gap of the $BiFeO_3$ nanostructures are lying in the visible region of the electromagnetic spectrum. Therefore this suggests that these nanostructures can found applications in photovoltaic. $BiFeO_3$ is direct energy band-gap (2.2–2.8 eV) semiconductor, chemically stable with high electron mobility and non-toxic. It is well known multiferroic material possessing simultaneously ferroelectricity, ferromagnetism or ferroelasticity in a single phase. Recently, it has been reported that $BiFeO_3$ thin film based-diode showing photovoltaic effects. More, importantly $BiFeO_3$ nanostructures are possessing

interesting photocatalytic activity in the visible region [36]. Numerous reports on the photocatalytic activities of $BiFeO_3$ are available as under:

Xiaomeng et al. reported two-dimensional $BiFeO_3$ plates, synthesized by hydrothermally. The average diameter and thickness of $BiFeO_3$ plates were about 1.3–2 lm and 200–300 nm. X-ray diffraction, scanning electron microscopy, UV–visible diffuse reflection spectrum were used to investigate the samples crystallinity, purity, morphology, spectral features. The effect of the morphology on photo-catalysis was also evaluated by photo-decolorization of orange II under a blended-light mercury fluorescent lamp. The results show that, $BiFeO_3$ plates showed a much higher photocatalytic activity than bulk $BiFeO_3$ for photo-decolorization of orange II, suggesting potential application in photo-catalysis [37].

Li et al. reported that $BiFeO_3$ uniform microcrystals with various morphologies were successfully synthesized by a controlled hydrothermal method. UV-vis spectra showed that the optical properties of the microsized $BiFeO_3$ crystals were strongly related to their shape and size. They further demonstrated the useful photocatalytic activity of these regular-shaped structures as determined by degradation of Congo red under visible-light irradiation ($\lambda > 400$ nm). Additionally, magnetic responses were observed to be influenced by the morphology of as-synthesized $BiFeO_3$ products, and the ferroelectric performance of $BiFeO_3$ submicrocube was also studied by piezoelectric force microscopy. Being a multiferroic semiconductor with suitable narrow band gap (~2.2 eV) and uniform morphologies, these $BiFeO_3$ microcrystals might be useful for the design of devices combining magnetic, electronic, and optical functionalities [38].

Huo et al. reported the $BiFeO_3$ non-titania photo-catalysts with instinct narrow energy gaps. $BiFeO_3$ represents a typical example owing to both the strong stability and the extremely narrow energy gap around 2.1 eV. Most $BiFeO_3$ samples have been synthesized by solid-state reactions, which exhibit poor activity due to the low surface area. However, the $BiFeO_3$ in solid particles and spindles also display poor light absorbance. Aerosol-spraying has been widely used for the rapid synthesis of nanomaterials with hierarchical structures. $BiFeO_3$ exhibits high activity attributed to the enhanced surface area favouring reactant adsorption and the increased light absorbance due to the multiple light reflections in the hollow chamber [39].

Li et al. reported the synthesis of anatase titania-coated bismuth ferrite nanocomposites ($BiFeO_3/TiO_2$) via a hydrothermal approach combined with a hydrolysis precipitation processing. Analysis of the microstructure and phase composition reveals that a core-shell $BiFeO_3/TiO_2$ structure can be formed, which results in a significant redshift in the UV-vis absorption spectra as compared to a simple

mechanical mixture of $BiFeO_3$–TiO_2 nanopowders. The core-shell structured $BiFeO_3/TiO_2$ nanocomposites exhibit higher photocatalytic activity for photo-degradation of Congo red under visible-light (λ>400 nm) irradiation, which should be attributed to the enhancement of the quantum efficiency by separating the electrons and holes effectively. The obtained $BiFeO_3/TiO_2$nanocomposites can be used as potential visible-light driven photo-catalysts [40].

Zhang et al. reported the heterostructures of thin titania films on $BiFeO_3$ substrates were grown by pulsed laser deposition. The heterostructures, when excited by visible light with energies between 2.53 and 2.70 eV, photo chemically reduce aqueous silver cations from solution in patterns that mimic the structure of the ferroelectric domains in the substrate. Under the same conditions, titania by itself reduces insignificant amounts of silver [41].

Lin et al. reported the *n*anostructured $BiFeO_3$ particles synthesized by a hydrothermal method, and the effects of particle size on photocatalytic activity and magnetic property of $BiFeO_3$ investigated. The optical absorption spectra indicate that the band-gap energy increases with decreasing crystalline size due to the quantum-size effect. The enhancement of room-temperature weak ferromagnetism can be observed in nanoscale $BiFeO_3$ particles, which should be attributed to the size-confinement effect on the magnetic ordering. In addition, BiFeO3 nanoparticles with diameter about 5 nm show good photocatalytic performance by photodegradation of Congo red under visible-light ($\lambda \gg 400$ nm) irradiation [42].

Madhu et al. reported sol-gel method synthesis of $Bi_{1-x}M_xFeO_3$ (M = Mg, Al, Y) ceramic materials. Subsequently, these materials were structurally characterized by applying Rietveld refinement techniques. The low band-gap nature of these materials enabled to them exhibit photocatalytic activity and accordingly 2% Y doped $BiFeO_3$ samples exhibited higher photocatalytic effect (18% compared to 14% for undoped). Under identical conditions, TiO_2 standard exhibited only 7% degradation indicating superior properties of cation-doped bismuth ferrites [43].

Feng et al. reported the synthesis of narrow-band gap semiconductor, $BiFeO_3$ by sol-gel method in ethanol. The photocatalytic activity of $BiFeO_3$ was researched with azo dye methyl orange solution as simulation sewage. The results show that $BiFeO_3$ is almost pure phase and semiconductor of band gap 2.03 eV, has the excellent visible-light photocatalysis. The $BiFeO_3$ will be a kind of new narrow-band gap semi semiconductor visible-light photocatalyst with broad application prospects [44].

Huo et al reports novel $BiFeO_3$ photocatalyst in the shape of uniform microspheres has been synthesized by solvothermal process assisted with chelating effect of citric acid. The higher photoactivity of this catalyst than that of $BiFeO_3$ via solid-state reaction for methylene blue (MB) degradation under visible-light irradiation is owing to the high crystallization of perovskite-type $BiFeO_3$, high surface area with

hollow structure, narrow band gap energy of 2.1 eV, and the promotion of separation of photo-induced electrons and holes. Additionally, no decrease of activity after being reused repetitively for five times is indicative of the high hydrothermal stability of $BiFeO_3$ particles without crystal phase transformation [45].

Xu et al. reported high surface area $BiFeO_3$ thin films were deposited on ITO substrates by templates method and chemical solution deposition. They further demonstrated the useful photocatalytic activity of these films as determined by degradation of Congo red under visible-light irradiation (λ>400nm). Their results showed that the surface area have a great effect on the photocatalytic performances of the $BiFeO_3$ thin films [46].

Wu et al. reported the hydrothermal synthesis of pure and rare earth elements (La, Yb)-doped $BiFeO_3$ microcrystallites. The results and analysis revealed that substitution of La and Yb not only changed the energy band gap of $BiFeO_3$ system, but also affected the morphologies and dimensions of $BiFeO_3$ microcrystallites. Despite much smaller particle size compared with pure $BiFeO_3$, the Yb-doped $BiFeO_3$ microcrystallites exhibited lower photocatalytic efficiency due to much larger energy band gap, which suggests the energy band configuration intensely influences the photocatalytic activity rather than the particle size [47].

Li et al. reported the hybrid photocatalysts consisting of single crystalline $BiFeO_3$ nanowires and laser ablated Au nanoparticles were synthesized by a functionalization-step-free solution process. The 1.0 wt% Au nanoparticle decorated $BiFeO_3$ nanowires exhibit 30 times higher photocatalytic activity for water oxidation than that exhibited by the parent wires during the first 4 h [48].

Li et al. reported $BiFeO_3$–graphene nanohybrids are fabricated via facile hydrothermal treatments. The morphology and band structure of $BiFeO_3$ are modulated by graphene. Nanohybrids with $BiFeO_3$ nanocrystallites of 100 nm uniformly decorated on graphene nanosheets are successfully synthesized, which exhibit a band gap of 1.78 eV. Significant enhancement in the visible light photocatalytic performance is achieved in the $BiFeO_3$–graphene nanohybrids. The rate for the photo-degradation of Congo Red under visible light is six times that for $BiFeO_3$ particles, which is attributed to the combined effects of modulated band gap and covalent bonding between $BiFeO_3$ and grapheme [49].

Ghaffari et al. reported vertically aligned TiO_2 nanorod arrays grown on FTO substrates by hydrothermal method. Different amounts of Au nanoparticles were deposited on the TiO_2 nanorods by photo reduction method. Au nanoparticles deposited TiO_2 nanorod DSSC have been fabricated and compared to cells built from TiO_2 nanorods without Au nanoparticles. From results it was found that Au nanoparticles deposited TiO_2 have presented significant improvements in fill factor and short circuit current, resulting

in as much as doubled overall conversion efficiencies. Au nanoparticles reduce recombination by forming a Schottky energy barrier that prevents photo injected electrons from approaching the surface of nanorod and improve the η from 0.31% (bare TiO_2 nanorod array DSSC) to 0.94% (Au nanoparticles deposited TiO_2 nanorod DSSC). VOC results confirmed that obtained samples are quite stable and no corrosion occurs between metal nanoparticles and the electrolyte. This study supports the application of Au nanoparticles TiO_2 nanorods in improving the performance of a DSSC [50].

Wen et al. generated the Ag island films by depositing the 3.3–6.0 nm-thick Ag nanoparticle layer on the TiO_2 film electrode using thermal evaporation and found a possibility of using plasmon resonance effect to enhance the efficiency of the DSSC [51].

Ihara et al. reported improved photoelectric conversion efficiency of DSSC by using localized surface plasmon of the Ag nanoparticles (diameter of 12.5 nm) modified with polymer and reported that the efficiency of DSSC with the Ag nanoparticles increased from 1.5% to 2.5% compared with the case with no Ag nanoparticles [52].

Nahm et al. reported the incorporated gold nanoparticles of 100 nm in diameter into TiO_2 nanoparticles for DSSC. At the optimum Au/TiO_2 mass ratio of 0.05, the power-conversion efficiency of the DSSC improved to 3.3% from a value of 2.7% without Au, and this improvement was mainly attributed to the photocurrent density. The Au nanoparticles embedded in the nanoparticulate-TiO_2 film strongly absorbed light due to the localized surface-plasmon resonance, and thereby promoted light absorption of the dye. In the DSSCs, the 100 nm-diameter Au nanoparticles generate field enhancement by surface-plasmon resonance rather than prolonged optical paths by light scattering [53].

Joshi et al. suggested that $BiFeO_3$ nanostructures can be used as photo-electrode material for DSSCs [54]. The above said properties, photocatalytic behavior and Joshi et al. suggesting superior photo-voltaic properties of $BiFeO_3$ nanostructures. This has been the motivation for the present study, to utilize metal deposit nanoparticles (Au and Cu) on $BiFeO_3$ nanostructures as photo-anode material in DSSCs.

In the light of above, it has been found that $BiFeO_3$ nanoparticles can be good candidates for the DSSC. More, importantly further enhancement in the energy-conversion efficiency can be achieved by the deposition of metal nanoparticles on the surface of $BiFeO_3$.

Recently, in light of above *Lotey et al.* reported new cue on dye-sensitized solar cells (DSSCs) fabricated using Gd-doped $BiFeO_3$ nanoparticles with particle size between 26-30 nm. The effect of Gd-doping and smaller size of synthesized nanoparticles on the structural, morphological, optical and photo-electrochemical properties have been investigated. The high energy-conversion efficiency, 3.85%, has been achieved for 12% Gd-doped $BiFeO_3$ DSSCs, which is more than 100% higher than the undoped

$BiFeO_3$. The possible origin of the observed performance of DSSCs has been explained on the basis of smaller size of the synthesized nanoparticles, doping of Gd and structural transformation with doping in $BiFeO_3$ [36].

Improvement of energy-conversion efficiency by deposition of metal nanoparticles on semiconductor

Metal nanoparticles are of great interest because of their unique electronic, optical, and magnetic properties. In particular, nanoparticles of noble metals such as gold and silver have been attracting more attention because they have many colors of varieties in the visible region based on plasmon resonance, which is due to the collective oscillations of the electrons at the surface of the nanoparticles. The resonance wavelength strongly depends on the size and shape of the nanoparticles, the inter-particle distance, and the dielectric property of the surrounding medium. The studies cited were concerned with only the increase in travel rate of the electrons. Less attention was paid to reduce the recombination of charges in the dye or electrolyte. Therefore, decreasing the recombination of charges in the dye or electrolyte is one of the most important considerations in increasing the conversion efficiency of DSSC, and is worthy of on-going study [50-53].

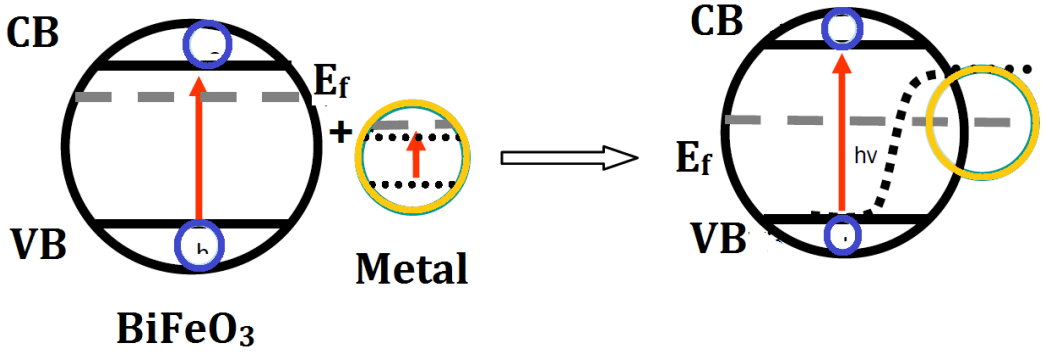

Figure 2.1: Fermi level equilibrium between $BiFeO_3$ and metal particles.

Deposition of metals is an effective way to improve the photovoltaic properties of semiconducting(Figure2.1). Therefore, deposition of selective elements offers an important route to enhance and control its optical and electrical properties, which is crucial to its practical applications.

It has been found that the deposition of metals (Au and Ag) on semiconductor TiO_2 nanoparticles is beneficial for maximizing the efficiency of photocatalytic reactions. This enhanced photocatalytic activity of TiO_2 is due to the shifting of Fermi energy level to negative potential leading to decrease in

potential difference between the conduction band of TiO_2 and the Fermi level of metal nanoparticles, hence facilitates charge transfer and reducing the charge recombination [50-53]. There are several reports available on photo-catalysis of metal (Au, Ag, Cu, Pt) deposited TiO_2 nanoparticles. It has been found that deposition of metals enhances the photo-catalytic activity.

The common methods for facilitating electron transfer from conduction band electrons to solution species has been through the use of metal island co-catalysts deposited onto the photocatalysis surface. These metal islands mediate multi-electron redox processes with solution phase redox carriers, and enhancement of both anodic and cathodic redox processes have been observed at illuminated semiconductor electrodes that have metal island deposits. Small metal islands of Ag, Au and Cu can be deposited onto the TiO_2 surface photo-chemically. Metal-semiconductor nanocomposites which results in the drastic increase in the activity of semiconductor by equilibrating the Fermi energy levels of both identities resulting in the easy transference of electrons from CB of semiconductor to metal. Deposition of metal on semiconductor enhances the efficiency of photocatalytic redox processes. Generally, the coinage metal nanoparticles are used for this purpose.

2.2 Gaps in the research:

From the literature review, it has been found that following area is not much explored:

As per the literature survey, no report is available on the performance of dye-sensitized solar cells based on metal deposited $BiFeO_3$ nanostructures.

2.3 Objectives:

Following are the objectives:

- Synthesis of $BiFeO_3$ nanoparticles by solution combustion method
- Deposition of Au metal on $BiFeO_3$ surface by photo-deposition method
- Characterization of the synthesized nanoparticles by X-ray diffraction (XRD), Transmission electron microscopy (TEM), UV-visible spectroscopy.
- Fabrication of dye-sensitized solar cells using as-synthesized nanoparticles
- Photovoltaic performance of fabricated DSSC.

Chapter-3

Synthesis and characterization techniques

3.1 Synthesis of Nanomaterials:

The nanomaterials can be prepared by different method categorized viz. Bottom up and Top down.

3.1.1 Top down approach

The top down approach often uses the traditional workshop or micro fabrication methods where externally controlled tools are used to cut, mill and shape materials into the desired shape and order, micro patterning techniques, such as photolithography and inkjet belong to this category.

Some examples of top-down approach:

1. Ball milling
2. Chemical vapor deposition
3. Electro-explosion
4. Laser ablation
5. Sputtering

3.1.2 Bottom up approach

A bottom up approach refers to the build-up of a material from the bottom i.e. atom by atom, molecule by molecule, or cluster by cluster. In crystal growth such as atoms, ions and molecules, after impinging onto the growth surface, assemble into crystal structure one after another. Although the bottom up approach is nothing new, it plays an important role in the fabrication and processing of nanostructure and nanomaterials. There are several reasons for this. When structures fall into a nanomaterial scale, there is little choice for top down approach. All the tools we have possessed are too big to deal with such tiny subjects. Bottom up approach is promising as compared to the top down approach because with this approach we can obtain nanostructures with fewer defects, more homogeneous chemical composition and better short and long range ordering. This is bottom up approach is driven mainly by the reduction of Gibbs free energy, so that nanostructures and nanomaterials such produced are in a state closer to a thermodynamic equilibrium state. On the contrary, top down approach most likely introduces internal

stress, in addition to surface defects and contaminations. Following are the examples of bottom up-approach:

1. Solution Combustion method
2. Sol-gel
3. Micro-emulsion
4. Reverse micelle
5. Chemical precipitation

In the present study, the Bismuth ferrite nanoparticles had been synthesized by solution combustion method. The detail of the experimental procedure is given below:

3.2 Solution combustion method

The solution combustion synthesis (SCS) of nanomaterials is a facile and economically viable technique for the preparation of advanced ceramics, catalysts and nanomaterials. It is characterized as high-temperatures, fast heating rates and short reaction times. These features make it an attractive method for the manufacture of technologically useful materials at lower costs compared to conventional ceramic processes. Some other advantages of SCS are:

i. Not require any sophisticated equipment, it is simple method
ii. High purity products can be synthesized
iii. Stabilization of meta-stable phases is possible
iv. Formation of virtually any size and shape products and high yield

There are two modes by which combustion synthesis can occur:

i. Self-propagating high-temperature synthesis (SHS)
ii. Volume combustion synthesis (VCS).

The characteristic feature of the SHS mode is, after initiation locally, the self-sustained propagation of a reaction wave through the heterogeneous mixture of reactants, followed by the synthesis of desired

condensed products. However, in the VCS, the entire sample is heated uniformly in a controlled manner until the reaction occurs essentially simultaneously throughout the volume, which leads to uniform microstructure and phase composition of the synthesized material. This mode of synthesis is more widely used for weakly exothermic reactions that require preheating prior to ignition, and is sometimes referred to as the thermal explosion mode**.**

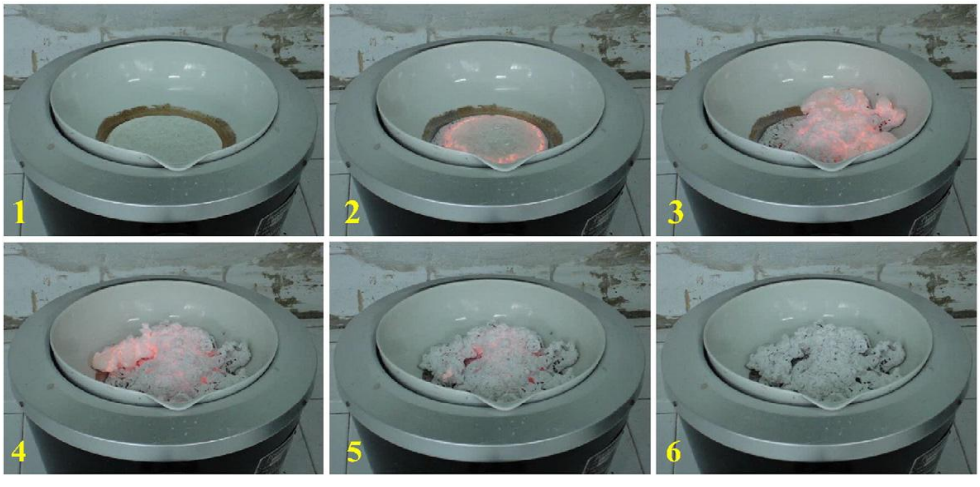

Figure 3.1: The evolution of solution combustion reaction [55]

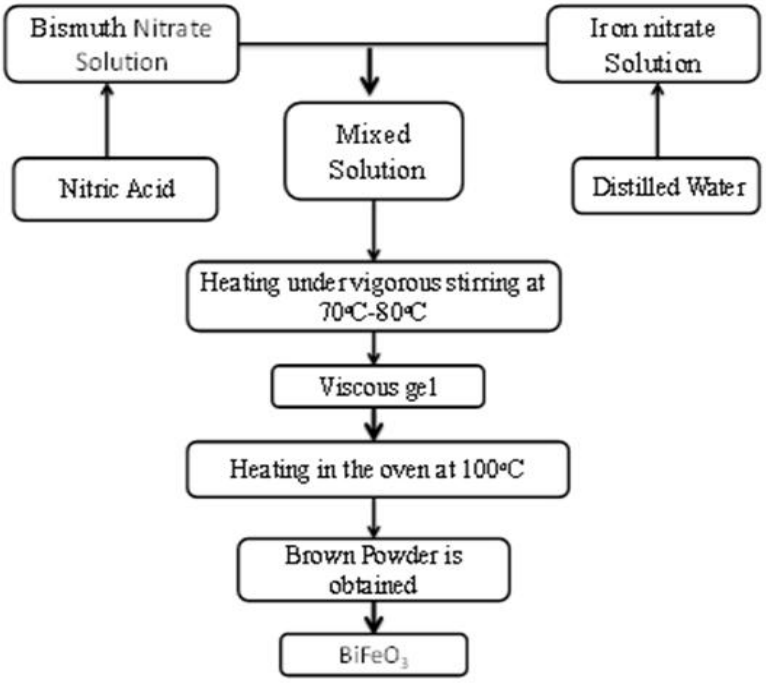

Figure 3.2: Schematic different steps involve in the synthesis of bismuth ferrite nanoparticles

3.3 Synthesis of $BiFeO_3$ nanoparticles by solution combustion method

The $BiFeO_3$ nanoparticles have been synthesized by solution combustion method. For the synthesis, the precursors used are bismuth nitrate ($Bi(NO_3)_3.5H_2O$), ferric nitrate ($Fe(NO_3)_3.2H_2O$), glycine ($C_2H_5NO_2$) and nitric acid (HNO_3). The de-ionized water is used as solvent. For the synthesis, the ferric nitrate ($Fe(NO_3)_3.2H_2O$) as well as bismuth nitrate ($Bi(NO_3)_3.5H_2O$) are dissolved in de-ionized water. The HNO_3 acid is added in the mixture of above solutions. Then the mixture is placed on the hot plate to evaporate solvent and other precursors. The fuel, glycine is added to the above solution. The temperature of the solution is kept at 70 °C -80°C. The detailed procedure is explained in Figure 3.2. After that the formation of gel takes place. Afterward, the solution ignites with a flame and the entire reaction was completed within 5 minutes. The powder obtained is of brown in color.

3.4 Deposition of gold (Au) on $BiFeO_3$ nanoparticles:

Metal nanoparticles are deposited on semiconductor by photodeposition technique. Charge transfer mechanism between semiconductor and metal nanoparticles is described as follows. The deposition of Au & Cu on the surface of synthesized $BiFeO_3$ nanoparticles have been done by photo- deposition method. In typical synthesis method, 2 weight % of $HAuCl_4$ is dissolved in ethanol separately.

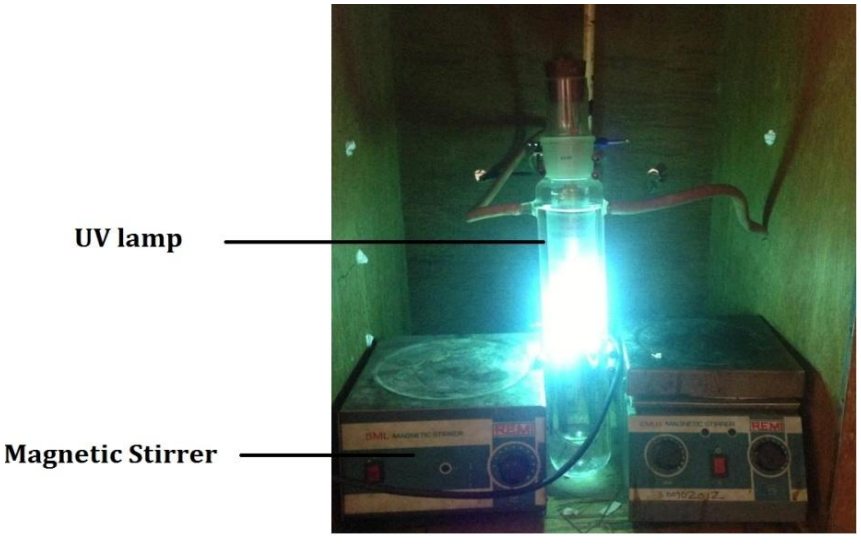

Figure 3.3 Photo-reactor used for the deposition of metal

These have been added in iso-propyl alcohol and water based solution of $BiFeO_3$ dispersed nanoparticles separately for Au & Cu. The argon gas has been purged in these solutions separately, and kept under the UV lamp for 2 h. The as-obtained samples were subsequently washed with distilled water dried and grounded [56]. Figure 3.3 shows the basic set-up used for the deposition of Au metal on $BiFeO_3$ surface. Figure 3.4 shows the idea and schematic of the metal deposition on the surface of $BiFeO_3$.

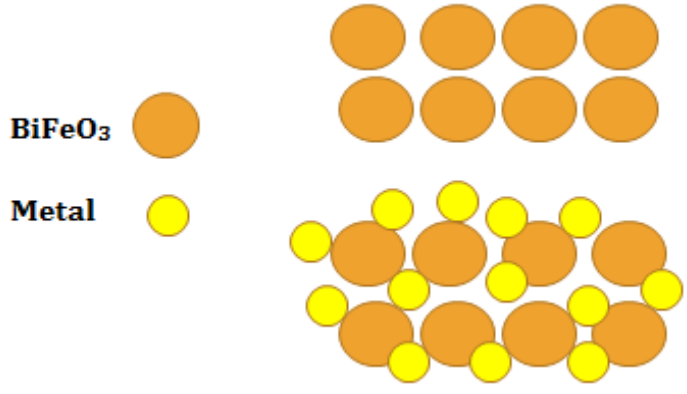

Figure 3.4: Deposition of metal on $BiFeO_3$ nanoparticles

3.5 Characterization techniques used

The synthesized nanoparticles have been characterized through different characterization techniques viz. XRD, TEM, UV-Visible spectroscopy, PL and JV characteristics to know their properties.

3.5.1 X-Ray diffraction

X-ray diffraction is a versatile, non-destructive method that reveals detailed information about the chemical composition, crystallographic and micro structure of all types of natural and manufactured materials. It is a valuable tool for the research and development of advanced materials. It provides information on structure, phase, preferred crystal orientations (texture) and other parameter such as average grain size, crystallinity, strain, crystal defects and crystallites size. The interaction of x-rays with sample creates secondary "diffracted" beams of x-rays related to interplanar spacing's in the crystalline powder according to a mathematical relation called Bragg's Law:

$$\mathbf{n\lambda = 2d \sin\theta}$$

where **n** is an integer, **λ** is the wavelength of the X-rays, **d** is the interplanar spacing generating the diffraction and **θ** is the diffraction angle. X-ray diffraction is based on the constructive interference of monochromatic X-rays and a crystalline sample.

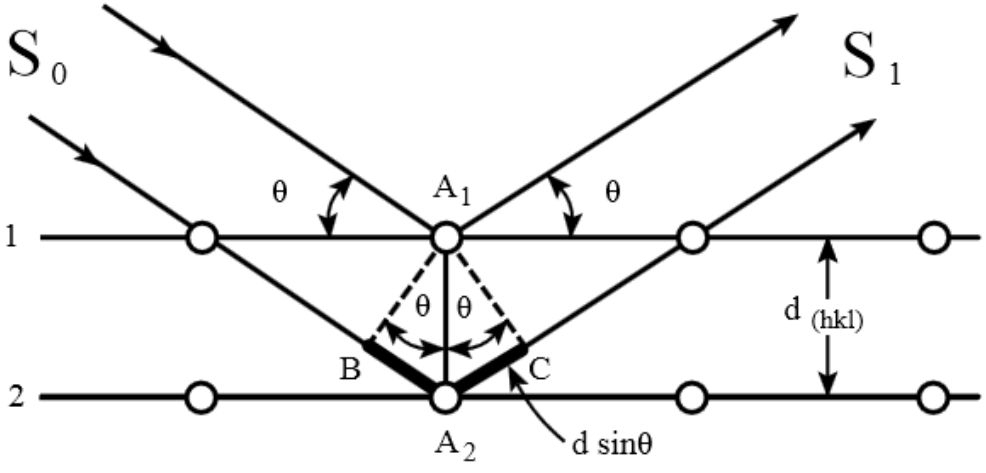

Figure 3.5: Schematic diagram of Bragg's diffraction from a set of parallel planes

These x-rays are generated by a cathode ray tube, filtered to produce monochromatic radiation, collimated to concentrate, and directed toward the sample. The figure 3.5 shows schematic of Bragg's diffraction from a set of parallel planes. The interaction of the incident rays with the sample produces constructive interference when conditions satisfy Bragg's law. This law relates the wavelength of electromagnetic radiation to the diffraction angle and the lattice spacing in a crystalline sample. These diffracted x-rays are then detected, processed and counted. The geometry of x-ray diffractometer is such that the sample rotates in the path of the collimated x-ray beam at an angle θ while the x-ray detector is mounted on an arm to collect the diffracted x-rays and rotates at an angle of 2θ. The lattice should be attained due to the random orientation of the powdered material. All diffraction methods are based on generation of X-rays in an X-ray tube.

3.5.2 Ultraviolet - visible spectroscopy

Ultraviolet-visible spectroscopy is an analytical technique that uses light in the visible, ultraviolet and near infrared ranges. UV-Vis spectroscopy refers to absorption spectroscopy in the ultraviolet-visible spectral region. In this region of the electromagnetic spectrum, molecules undergo electronic transitions. The absorption of light occurs very quickly femto-second time scale. The energy in a quantum (Planck's Law) is expressed by the equation:

$E = h\nu = hc/\lambda$

where E is the energy, h is Planck's constant, **ν** and **λ** are the frequency and wavelength of the incoming photon, and **c** is the speed of light.

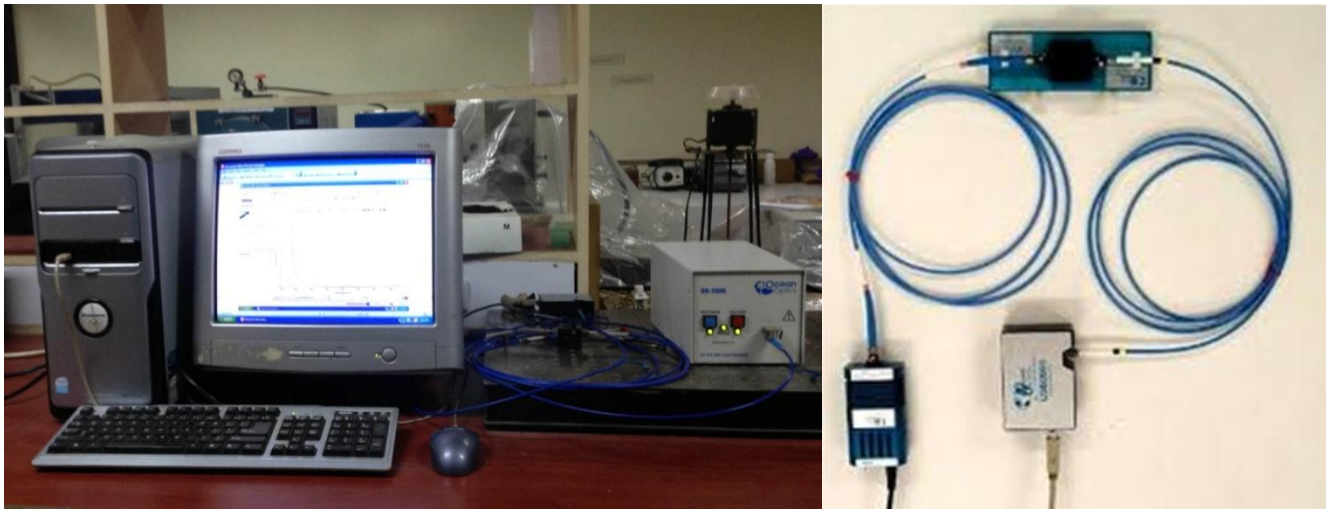

Figure 3.6: Experimental set of UV-visible spectrometer used

The wavelength of light that a compound will absorb is characteristic of its chemical structure.

Specific regions of the electromagnetic spectrum are absorbed by exciting specific types of molecular and atomic motion to higher energy levels. Absorption of visible and ultraviolet (UV) radiation is associated with excitation of electrons, in both atoms and molecules, to higher energy states. All molecules will undergo electronic excitation following absorption of light, but for most molecules very high energy radiation (in the vacuum ultraviolet, <200 nm) is required. For molecules containing conjugated electron systems however, light in the UV-visible region is adequate. As the degree of conjugation increases, the spectrum shifts to lower energy.

3.5.3 Transmission electron microscopy (TEM)

Transmission electron microscopy (TEM) is a microscopy technique whereby a beam of electrons is transmitted through an ultra-thin specimen, interacting with the specimen as it passes through. An image is formed from the interaction of the electrons transmitted through the specimen; the image is magnified and focused onto an imaging device, such as a fluorescent screen, on a layer of photographic film, or to be detected by a sensor such as a CCD camera. TEMs are capable of imaging at a significantly higher resolution than light microscopes, owing to the small de Broglie wavelength of electrons. This enables the instrument's user to examine fine detail—even as small as a single column of atoms, which is tens of

thousands times smaller than the smallest resolvable object in a light microscope. TEM forms a major analysis method in a range of scientific fields, in both physical and biological sciences.

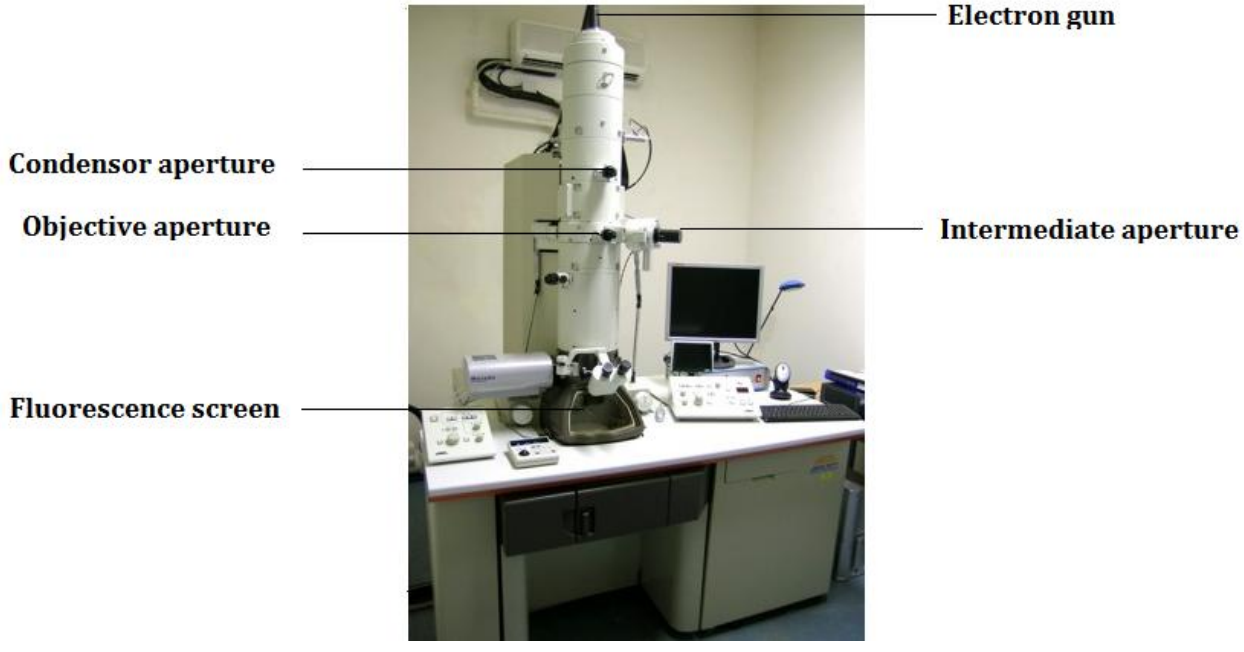

Figure 3.7: Layout of TEM

At smaller magnifications TEM image contrast is due to absorption of electrons in the material, due to the thickness and composition of the material. At higher magnifications complex wave interactions modulate the intensity of the image, requiring expert analysis of observed images. Alternate modes of use allow for the TEM to observe modulations in chemical identity, crystal orientation, electronic structure and sample induced electron phase shift as well as the regular absorption based imaging. The TEM is composed of several components, which include a vacuum system in which the electrons travel an electron emission source for generation of the electron stream, a series of electromagnetic lenses, as well as electrostatic plates (Figure 3.7). The latter two allow the operator to guide and manipulate the beam as required. Also required is a device to allow the insertion into, motion within, and removal of specimens from the beam path. Imaging devices are subsequently used to create an image from the electrons that exit the system. TEM find application in various field such as for morphological analysis, electronic diffraction.

3.5.4 Photo-electrochemical analysis

3.5.4.1 Current density-applied voltage (J-V) characteristics of DSSC

There are several methods to determine the parameters of the solar cells. One of the key measurements needed for photovoltaic devices in the measurement of their current density-applied voltage (J-V) characteristics. Through these, we can determine physical performances of DSSC uch as photo-electric conversion efficiency, fill factor. Figure 3.8 shows the typical JV characteristics curve. Different parameters that can be calculated from JV curves:

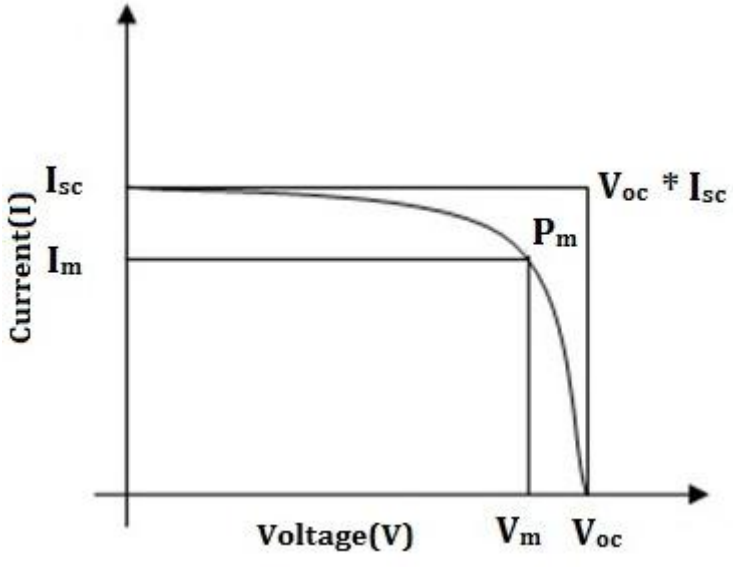

Figure 3.8: Current-voltage characteristics of the solar cell

Short-circuit current (Isc) is the current through the solar cell when the voltage across the solar cell is zero. The short-circuit current is due to the generation and collection of light-generated carriers. For an ideal solar cell at most moderate resistive loss mechanisms, the short-circuit current and the light-generated current are identical. Therefore, the short-circuit current is the largest current which may be drawn from the solar cell.

Open-circuit voltage (V_{OC}) is the maximum voltage available from a solar cell, and this occurs at zero current. The open-circuit voltage corresponds to the amount of forward bias on the solar cell due to the bias of the solar cell junction with the light-generated current. The short-circuit current and the open-circuit voltage are the maximum current and voltage respectively from a solar cell. However, at both of these operating points, the power from the solar cell is zero.

Fill factor (FF) is a parameter which, in conjunction with Voc and Isc, determines the maximum power from a solar cell. The FF is defined as the ratio of the maximum power from the solar cell to the product of Voc and Isc. Graphically, the FF is a measure of the "squareness" of the solar cell and is also the area of the largest rectangle which will fit in the IV curve. The maximum theoretical FF from a solar cell can

be determined by differentiating the power from a solar cell with respect to voltage and finding where this is equal to zero. Therefore,

$$\frac{d(IV)}{dV} = 0$$

This giving: $V_{MP} = V_{OC} - \frac{nkT}{q} \ln\left(\frac{V_{mp}}{nkT/q} + 1\right)$

This equation above only relates Voc to Vmp. The expression for the FF can be determined as:

$$FF = \frac{V_{OC} - \ln(V_{OC} + 0.72)}{V_{OC} + 1}$$

where Voc is defined as: $V_{OC} = \frac{q}{nkT} V_{OC}$

Energy conversion efficiency (η) is the most commonly used parameter to compare the performance of one solar cell to another. Efficiency is defined as the ratio of energy output from the solar cell to input energy from the sun.The efficiency of a solar cell is determined as the fraction of incident power which is converted to electricity and is defined as:

$$P_{max} = V_{OC} I_{sc} FF$$

$$\eta = \frac{V_{Oc} I_{SC} FF}{P_{in}}$$

Chapter - 4

Results and discussion

4.1 Structural analysis

For the structural analysis of the synthesized nanoparticles, X-ray diffraction (XRD) study has been carried out. Figure 4.1 and 4.2 show the XRD patterns of bare $BiFeO_3$ and Au-deposited nanoparticles respectively.

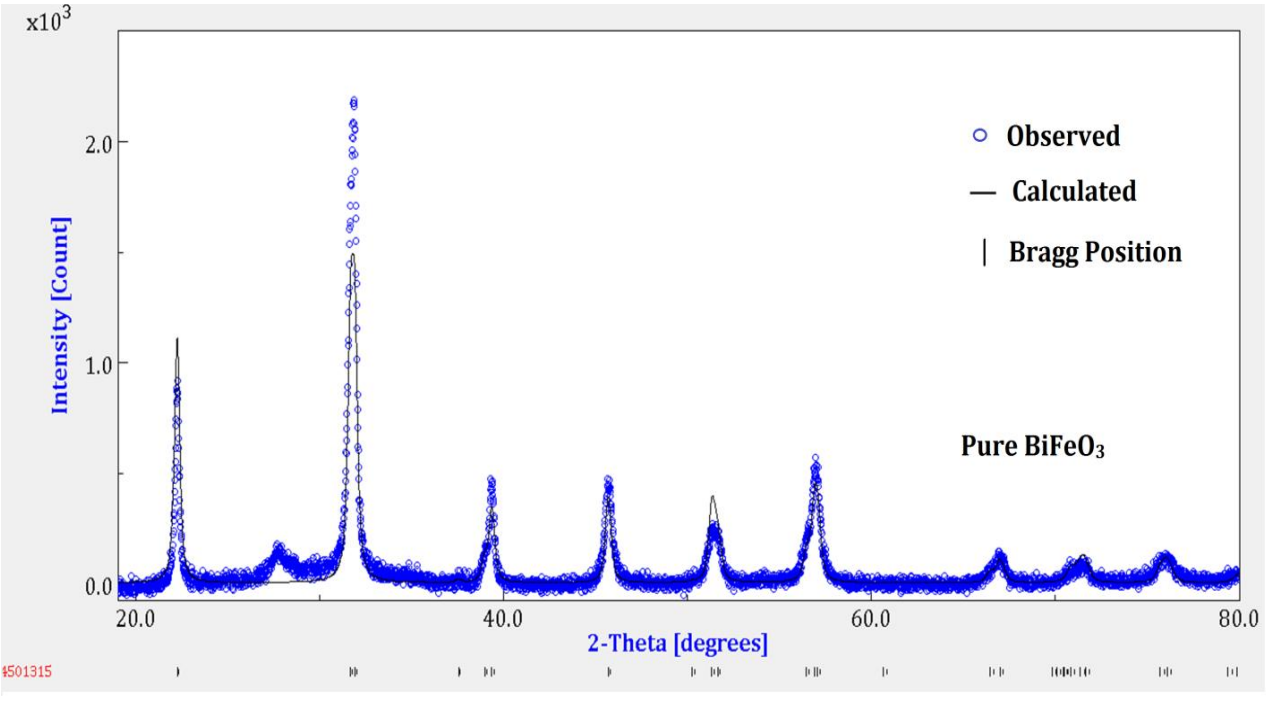

Figure 4.1: XRD patterns of bare $BiFeO_3$ nanoparticlesTo carried out detailed structural analysis

Rietveld analysis of the XRD patterns have been performed using FullProf program. The observed, calculated and the different refined XRD patterns of the synthesized nanoparticles are shown in Figure 4.1 and 4.2. It has been found that the XRD patterns of synthesized $BiFeO_3$ nanoparticles are well agreement with hexagonal phase of rhombohedral structure with R3*c* space group (JCPDS file no. 86–1518). No peak related to Au or any other compound has been found in the XRD patterns. The average crystallite size for bare and Au-deposited $BiFeO_3$ nanoparticles has been found to be found to be 46 nm and 26 nm, respectively. No additional peaks related to any impurity or other phases have been detected in XRD patterns revealing their defect-free nature without the formation of any secondary phase. The high intense peaks of XRD patterns demonstrate the high crystalline nature of the synthesized nanoparticles.

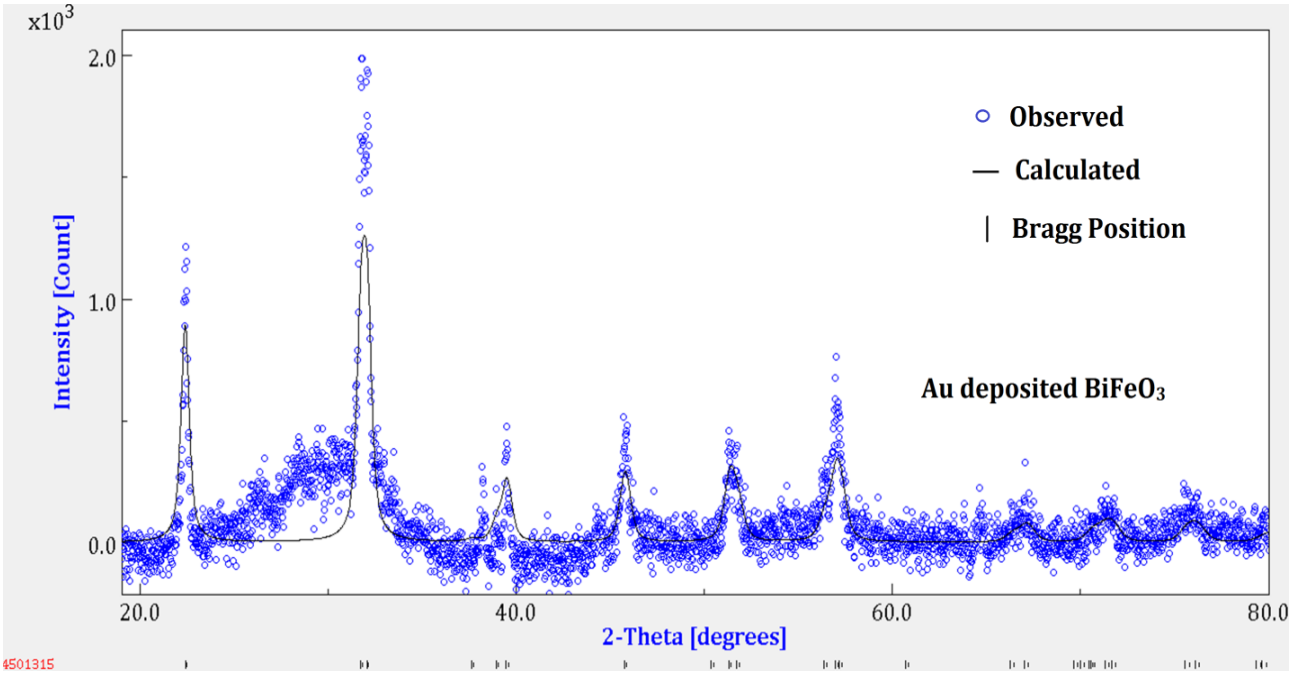

Figure 4.2: XRD patterns of Au-deposited $BiFeO_3$ nanoparticles

4.2 Morphological study

The morphological study of the synthesized $BiFeO_3$ has been carried out using TEM. Figure 4.3 shows the TEM image of pure $BiFeO_3$, revealing their spherical morphology. The synthesized nanoparticles are found to be in agglomeration state due to magnetic nature of nanoparticles. The average particle size has been found to be around 56 nm. Figure 4.4 shows the TEM image of the Au-deposited $BiFeO_3$ nanoparticles. It has been found from the TEM image that the Au nanoparticles have been successfully deposited on the surface of $BiFeO_3$ nanoparticle marked by arrows. This confirms the Au-deposition on the surface of $BiFeO_3$ nanoparticles. The size of the Au-deposited $BiFeO_3$ found to be 28 nm.

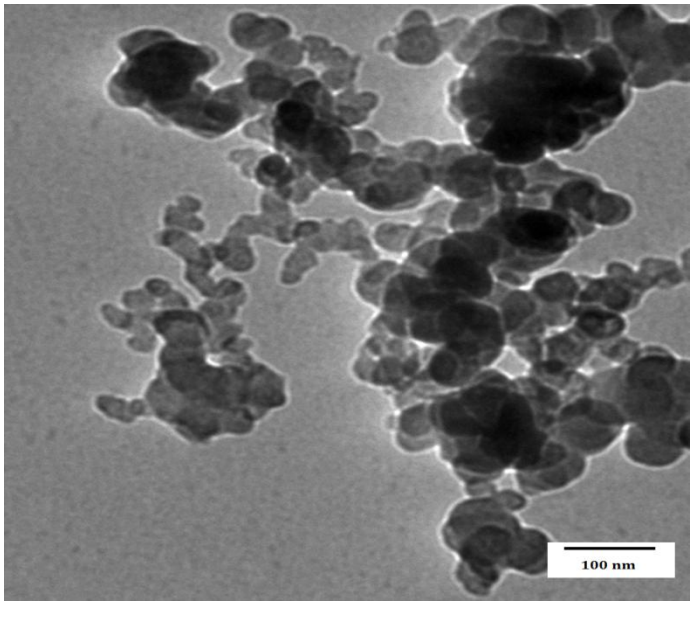

Figure 4.3: TEM images of bare $BiFeO_3$ nanoparticles

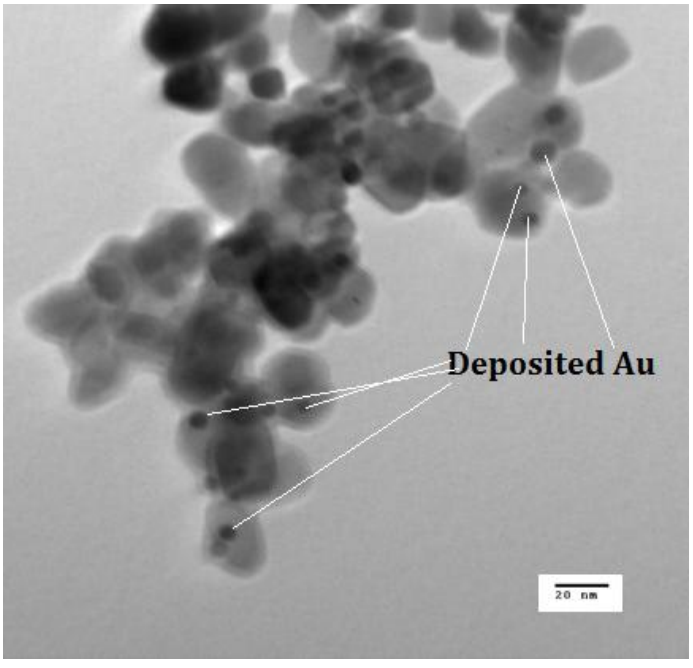

Figure 4.4: TEM images of Au deposited $BiFeO_3$ nanoparticles

4.3 UV-visible absorption study

UV-visible reflectance spectra of synthesized samples have been measured and transformed into absorption spectra using Kubelka-Munk method as shown in Figure 4.5. The band gap of the synthesized nanoparticles of Au-deposited $BiFeO_3$ nanoparticles has been found to be 2.28 eV. This demonstrates synthesized $BiFeO_3$ nanoparticles as direct band gap semiconductor. It has been found that the band gap of the synthesized nanoparticles shows blue shift. The observed blue shift in the band gap can be attributed quantum confinement results due to smaller size of synthesized nanoparticles that lead to the localization of electrons and holes in the semiconductor nano-crystallites [38]. In addition to this, the broad absorption band edge has been observed (Figure 4.5) in the range of 350 - 500 nm. This can be attributed to two types of electronic transitions, i.e., first from $^6A_1 \rightarrow {}^4T_1$, $^6A_1 \rightarrow {}^4E$, $^4A_1(^4G)$ ligand field and field transfer transitions overlap with each other resulting in a broadband, and second associated with d-d transitions (charge transfer transitions) of Fe^{3+} ions from $^6A_1$ to $^4E(^4D)$ and $^4T_2(^4D)$ level [1]. The UV-visible spectra study shows that the synthesized nanoparticles absorb light in visible-region, therefore may be useful to in photovoltaic or optoelectronic devices.

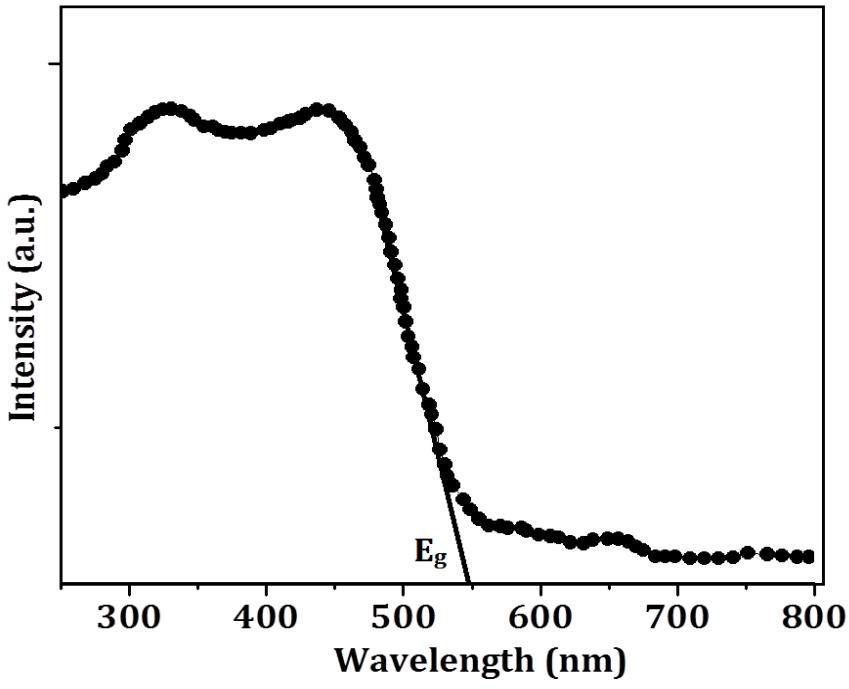

Figure 4.5 UV-visible diffuse reflectance spectra of Au-deposited $BiFeO_3$ nanoparticles

4.4 Photochemical analysis

4.4.1 Fabrication of DSSC using synthesized $BiFeO_3$ nanoparticles

The working electrodes for DSSCs have been fabricated using synthesized nanoparticles by doctor blade technique with 0.5x0.5cm^2 film area. In typical procedure, the fabricated electrodes were sintered at 450^oC for 30 minutes. After cooling, the electrodes were immersed into the dye solution (0.3mM, N719 dissolved in ethanol) and kept at room temperature for 60 h for complete dye adsorption.

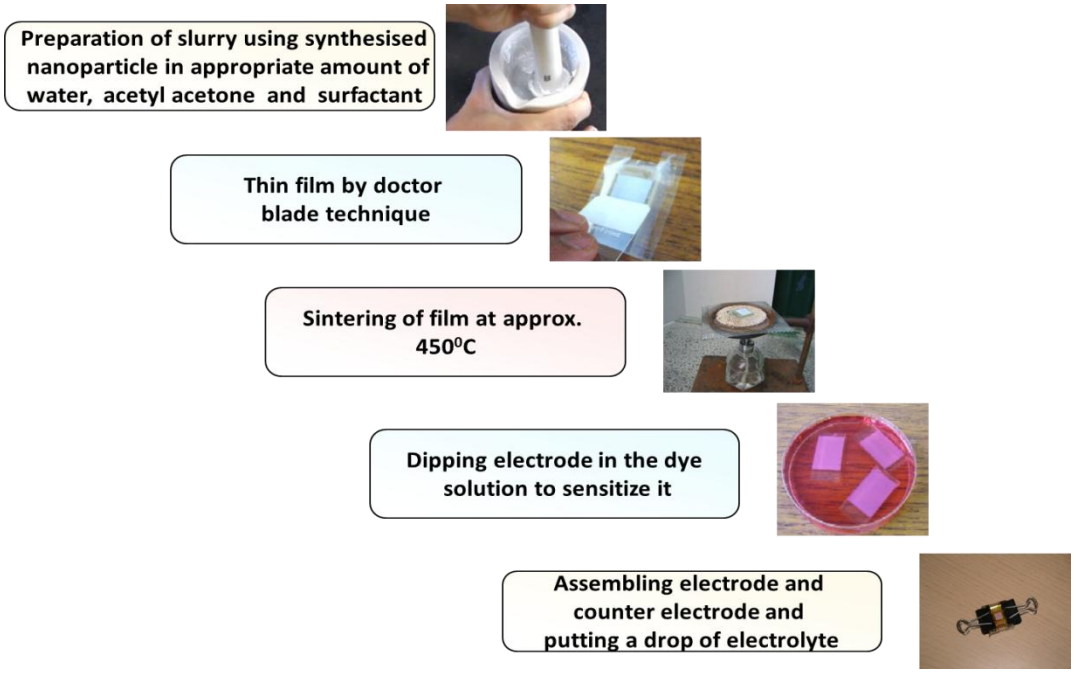

Figure 4.6: Different steps involve in the fabrication of the DSSC

The Pt-counter electrode was fabricated by spin coating a drop of chloroplatinic acid hexahydrate (5 mM in isopropanol solution) on the FTO glass, and, further heating it at 400^{o}C for 15 min. The dye-covered electrodes and Pt-counter electrode were assembled into a sandwich-type cell. A few drops of electrolyte solution (0.1M LiI, 0.05M I2, 0.3M 1,2-dimethyl-3-propyl imidazolium iodine, and 0.5M tert-butylpyridine in 3-methoxypropionitrile) were injected in between the assembled DSSCs. Photocurrent density-voltage (J-V) curve measurements were recorded by employing a 1000W Oriel solar simulator (equipped with an AM1.5 filter, Newport, 81094) attached with Keithley (2420) digital source meter.

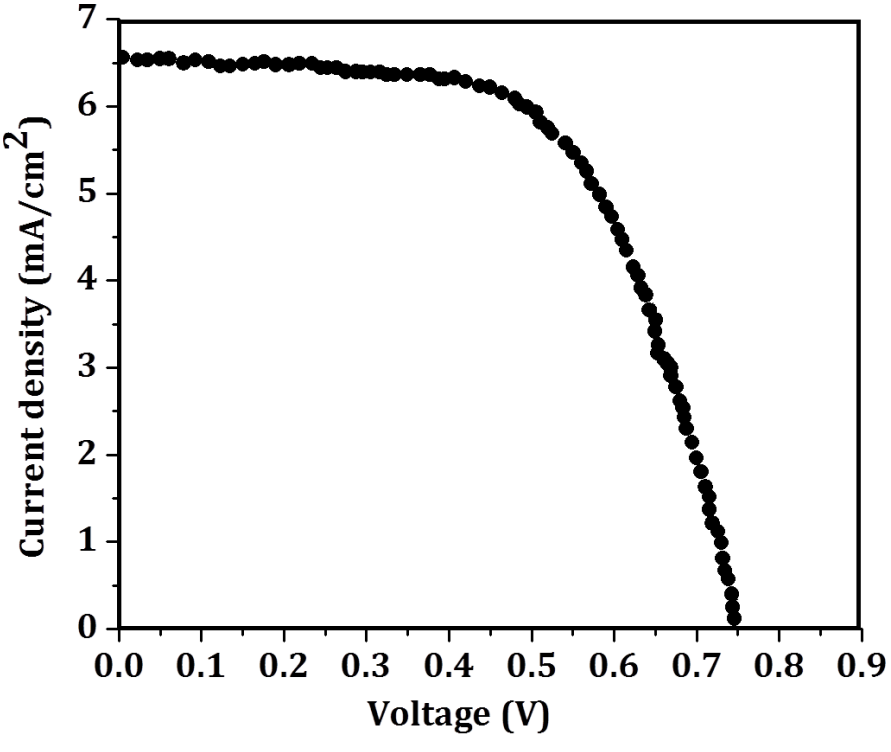

Figure 4.7: Photo-current density versus applied voltage characteristics curves of dye-sensitized solar cells

4.4.2 Photovoltaic performance of the fabricated DSSC

Figure 4.7 shows the photocurrent density versus applied voltage (J-V) characteristics curves of the fabricated DSSCs. Table 1 summarized the different performance parameters of fabricated DSSCs viz. open-circuit voltage (V_{OC}), short circuit current-density (J_{SC}), fill factor (FF) and efficiency (η) calculated from the J–V curves. The efficiency of the fabricated DSSCs has been found to be 2.99 % which is higher than our previous report for the bare $BiFeO_3$ [36]. The Au-deposition acts as to prevent charge carrier recombination by forming a Schottky energy barrier. This promotes the photo-injected electrons into the nanoparticles, away from the surface, which improves the overall conversion efficiency of the DSSCs

compared to our previous report [36]. This study establishes that the Au-deposited $BiFeO_3$ nanoparticles can be used for designing of high-performance DSSCs and photovoltaic devices.

Table 1 Performance parameters of DSSCs based on undoped and Au-deposited $BiFeO_3$ electrodes

Sample Description	Crystallite Size(nm)	Band Gap(eV)	J_{sc} (mA/cm^2)	V_{oc}(V)	FF (%)	η %
Au-deposited $BiFeO_3$ nanoparticle	26	2.28	6.5	0.75	0.62	2.99

Chapter – 5
Conclusions and future scope

5.1 Conclusions

- $BiFeO_3$ nanoparticles of have been synthesized by solution combustion method.
- The deposition of Au on the surface of $BiFeO_3$ has been done using photo-deposition method.
- X-ray diffraction confirms that the synthesized nanoparticles are possessing rhombohedral structure with hexagonal phase having space group R3*c*.
- The average crystallite size for bare and Au-deposited $BiFeO_3$ nanoparticles has been found to be found to be 46 nm and 26 nm, respectively.
- TEM image of pure $BiFeO_3$, revealing their spherical morphology. The synthesized nanoparticles are found to be in agglomeration state due to magnetic nature of nanoparticles. The average particle size has been found to be around 56 nm
- TEM image of the Au-deposited $BiFeO_3$ nanoparticles confirms the deposition of Au on the surface of $BiFeO_3$ nanoparticle. The size of the Au-deposited $BiFeO_3$ found to be 28 nm.
- Synthesized nanoparticles possess band gap 2.28 eV, in the visible region. In addition to this, the broad absorption band edge has been observed in the range of 350 - 500 nm. This can be attributed to two types of electronic transitions, i.e., first from $^6A_1 \rightarrow {}^4T_1$, $^6A_1 \rightarrow {}^4E$, $^4A_1(^4G)$ ligand field and field transfer transitions overlap with each other resulting in a broadband, and second associated with d-d transitions (charge transfer transitions) of Fe^{3+} ions from $^6A_1$ to $^4E(^4D)$ and $^4T_2(^4D)$ level.
- The dye-sensitized solar cells (DSSCs) have been fabricated using synthesized nanoparticles. The effect of Au-deposition on photovoltaic performance of DSSCs has been investigated.
- The different performance parameters of fabricated DSSCs viz. open-circuit voltage (V_{OC}), short circuit current-density (J_{SC}) and fill factor (FF) found to be 0.75 V, 6.5 mA/cm^2, 0.62, respectively. The high energy-conversion efficiency, 2.99%, has been achieved in Au-deposited $BiFeO_3$ based DSSCs.

5.2 Future Scope

To enhance the energy conversion efficiency of the synthesized nanoparticles, numerous factors such as deposition of other coinage metals, doping of rare earth metals, fabrication of different morphologies can be done.

The different parameters such as dye, thickness of films and size of the nanostructures can be optimized to get maximum efficiency.

References

[1] M. Grätzel, Acc. Chem. Res., 42, 1788– 1798 (2009).

[2] L. M. Bharadwaj, V. Bhalla, Nanoparticles for pharmaceutical applications, American Scientific Publisher, USA, 177-190 (2007).

[3] L.M. Bharadwaj, A.P. Bhandekar, A.K.Shukla, V.Bhalla, R.P. Bajpai, SPIE, 4397, 319-325 (2003).

[4] S. Kumar, S.K.Chakarvati, Digest Journal of Nanomaterials and Biostructures, 1(4), 139-143 (2006).

[5] http://org.ntnu.no/solarcells/pages/generations.php

[6] M.A. Green, Prog. Photovolt: Res. Appl.9:123-135 (2001).

[7] G. Cao, Nanostructures and Nanomaterials (Imperial College Press, London) (2004).

[8] T. Soga, Nanostructured Materials for Solar Energy conversion, Elsevier, Japan (2006).

[9] B. O'Regan, M Grätzel, Donald Fitzmaurice, Chem.Phy.Lett., 183, 89-93(1991)

[10] Martin A. Green,Keith Emery,Yoshihiro Hishikawa, Wilhelm Warta, Ewan D. Dunlop, Prog in photovolt.12–20, (2012).

[11] Chun, K.Y.; Park, B.W.; Sung, Y.M.; Kwak, D.J.; Hyun, Y.T.; Park, M.W. *Thin Solid Films*, 517 (14) 4196-4198 (2009)

[12] M. Zhong, Jingying Shi, Wenhua Zhang, Hongxian Han, Can Li,Charge, J. Mater. Sci. Eng, B 176, 1115–1122 (2011).

[13] K. Tennakone, G. Kumara, I.R.M. Kottegoda, V.P.S. Perera, Chem. Commun,32,15-16 (1999).

[14] K. Keis, E. Magnusson, H. Lindstrom, S.E. Lindquist, A. Hagfeldt, Mater. Sol. Cells 73,51-58 (2002).

[15] P. Guo, M.A. Aegerter, Thin Solid Films, 351,290-294 (1999).

[16] B. Tan, E. Toman, Y.G. Li, Y.Y. Wu, J. Am. Chem. Soc., 129,4162 (2007).

[17] E. Serrano, G. Rus,Renew. Sustain. Energy , Rev. 13, 2373 (2009).

[18] Vlachopoulos, N.Liska, P.Augustynski, J.Gratzel, J. Am. Chem. Soc., 110, 1216–1220 (1988).

[19] A. Hauch, A. Georg, U.O. Krasovec, B. Orelc, J. Electrochem. Soc.9, H159–H163 (2002).

[20] Y. Gao, M. Nagai, Langmuir, 22, 3936-3940 (2006).

[21] C. H. Ku, J. J. Wu, Nanotechnology, 18, 505706 (2007).

[22] A. B. F. Martinson, J. W. Elam, J. T. Hupp, M. J. Pellin, Nano letters, 7, pp 2183–2187 (2007).

[23] Y. Ohsaki, N. Masaki, T. Kitamura, Y. Wada, T. Okamoto, T. Sekino, K. Niihara, S Yanagida, Phys. Chem. Chem. Phys., 7, 4157-4163 (2005).

[24] C. Y. Jiang, X. W. Sun, G. Q. Lo, D. L. Kwong, J. X. Wang, Appl. Phys. Lett., 90, 263501 (2007).

[25] I. C. Baek, M. Vithal, J. A. Chang, J. H. Yum, M. K. Nazeeruddin, M. Grätzel, Y. C Chung, S. I. Seok, Electrochem. Comm.11, 909–912 (2009).

[26] H. Wang, Y. Liu, M. Li, H. Huang, M. Zhong, H. Shen, Appl Phys A, 97, 25–29 (2009).

[27] Y. F. Hsu, Y. Y. Xi, C. T. Yip, A. B. Djurisic, W. K. Chan, J. Appl. Phys., 103, 083114 (2008).

[28] S. S. Kim, J. H. Yum, Y. E. Sung, J. Photochem. Photobio, 171, 269-273 (2005).

[29] D. B. Menzies, R. Cervini, Y. B. Cheng, G. P. Simon, L. Spiccia, J.Sol-gel. Sci. Tech., 32, 363–366 (2004).

[30] D.B Menzies, L. Bourgeois, Y. B. Cheng, G. P. Simon, N. Brack, L. Spiccia, Surface and Coatings Tech., 198, 118-122 (2005).

[31] Y. Diamant, S. Chappel, S. G. Chen, O. Melamed, A. Zaban, Coord. Chem. Rev., 248, 1271-1276 (2004).

[32] S. G. Chen, S. Chappel, Y. Diamant, A. Zaban, Chem. Mater.,13, 4629-4634 (2001).

[33] Y. Diamant, S. G. Chen, O. Melamed, A. Zaban, Core J. Phys. Chem. B, 107,1977-1981 (2003).

[34] J. Y. Kim, S. Lee, J. H. Noh, H. S. Jung, K. S. Hong, J Electroceram., 23, 422-425 (2009).

[35] S. Lee, J. Y. Kim, K. S. Hong, H. S. Jung, J. K. Lee,H. Shin, Solar Energy Mat. & Solar Cells, 90, 2405–2412 (2006).

[36] G.S. Lotey, N.K. Verma, Chem Phys Lett, 574, 77 (2013).

[37] L. Xiaomeng, Xie Jimin, Song Yuanzhi, Lin Jiamin, J. Mat.Sci. 42 (6) 6824-6827 (2007).

[38] S. Li, Y. H. Lin, Bo-Ping Zhang,Yao Wang, Ce-Wen Nan , J. Phys. Chem. C 114, 2903–2908 (2010).

[39] Y. Huo , Miao Miao , Yi Zhang , Jian Zhu,Hexing Li, Chem. Commun., **47**, 2089-2091 (2011).

[40] S. Li, Y.H. Lin, B.P. Zhang, Jing-Feng Li, CW Nan, J. Appl. Phys. 105, 054310 (2009).

[41] Yiling Zhang , Andrew M. Schultz , Paul A. Salvador, Gregory S. Rohrer, J. Mater. Chem., 2011, 21, 4168-4174 (2011).

[42] Lin, Yuan-Hua, Zhang, Bo-Ping , Nan, Ce-Wen ,J.App.Sci.(2009).

[43] Madhu, C Bellakki, Manjunath B, Manivannan, V, IJEMS Vol.17(2) (2010).

[44] C. Feng, T. Peisong, C. Haifeng, P. Guoxiang **,** Rare metal Mat. Engg.(2010).

[45] Y. Huo, Y.Jin, Y. Zhang , J. Mol. Catalysis.(2010).

[46] X. Xu, Y.H. Lin, Pai Li, Li Shu,Ce-Wen Nan, J. Am. Cer. Soc.8,2296-2299 (2011).

[47] C. Wu, J Wei, F Kong, J Mater Sci, 24,1530–1535 (2013).

[48] S. Li, J. Zhang, M. G. Kibria, Z. Mi, M. Chaker, D.Ma, R. Nechache, F. Rosei, Chem. Commun.,(2013).

[49] Z. Li, Y. Shen, C. Yang, Y. Lei, Y. Guan, Y. Lin, D. Liu, C.W. Nan, J. Mater. Chem. *A*,**1**, 823-829 (2013).

[50] M. Ghaffari, et al., Electrochim Acta,76,446-452 (2012).

[51] C. Wen, K. Ishikawa, M. Kishima, K. Yamada, Solar Energy Mat. Solar Cells,61, 339–351 (2000).

[52] M. Ihara, M. Kanno, S. Inoue, Physica E, 42, 2867–2871 (2010).

[53] T. Y. Chen, C. M. Fan, J. Y. Wu, and T. L. Lin, J. Chinese Chem. Soc.1244–1249 (2009).

[54] U.A. Joshi, J.S. Jang, P.H. Borse, J.S. Lee, Appl. Phys. Lett. 92 242106 (2008).

[55] R. Ianos, L. Lazau, C. Pacurariu, P. Barvinschi, Cem.Concrete Research,39, 7, 566-572, (2009).

[56] R. Kaur, B. Pal, J. Mol. Catalysis, 355, 39– 43 (2012).